Title
Getters for improved technetium containment in cementitious waste forms.

Authors
Asmussen, R Matthew
Pearce, Carolyn I
Miller, Brian W
et al.

Publication Date
2018

DOI
10.1016/j.jhazmat.2017.07.055

Peer reviewed

Getters for Improved Tc Containment in Cementitious Waste Forms

R. Matthew Asmussen[1], Carolyn I. Pearce[1], Brian D. Miller[1], Amanda R. Lawter[1], James J. Neeway[1], Wayne W. Lukens[2], Mark Bowden[1], Micah Miller[1], R. Jeffery Serne[1], Nikolla P. Qafoku[1]

[1]Pacific Northwest National Laboratory, Richland, WA

[2]Chemical Sciences Division, Lawrence Berkeley National Laboratory, Berkeley, CA

Keywords : nuclear waste management, technetium, getters, cementitious, grout, radiography, spectroscopy

Abstract

Cementitious waste forms present a low-temperature, low-cost option for the immobilization of nuclear wastes. At the U.S. Department of Energy Hanford Site, the low activity waste (LAW) portion of the nuclear wastes stored at the site will contain Tc-99, a long lived radionuclide capable of high environmental mobility. A cementitious waste form known as Cast Stone is under investigation as a possible candidate technology for the immobilization of LAW. Ensuring slow rates of release of Tc from a LAW waste form, be it glass or cementitious, is essential for safe disposal of the waste. This work focuses on the addition of getter materials to Cast Stone that can selectively immobilize Tc from the LAW, and in turn, lower Tc release from the Cast Stone. Two getters which produce different products upon sequestering Tc from LAW were tested in Cast Stone; Sn(II)-treated apatite (Sn-A) which removes Tc as a Tc(IV)-oxide and potassium metal sulfide (KMS-2) which removes Tc as a Tc(IV)-sulfide species. The Cast Stone treated with KMS-2 had the largest impact. The observed diffusion (D_{obs}) of Tc decreased from $4.6 \pm 0.2 \times 10^{-12}$ cm^2/s for Cast Stone that did not contain a getter to $5.4 \pm 0.4 \times 10^{-13}$ cm^2/s for KMS-2 containing Cast Stone, where KMS-2 addition was equivalent to < 0.01 wt% of the total waste form mass. The Sn-A Cast Stone also improved Tc D_{obs} over time, however initial releases were higher due to the higher level of Sn-A addition required (~ 2 wt% overall). Spectroscopic investigations using single particle digital autoradiography and μ-X-ray fluorescence determined Tc to remain associated with the getter materials within the Cast Stone matrix. It was found that Tc-sulfide species are more stable within Cast Stone compared with Tc-oxides using x-ray absorption spectroscopy (XAS). This stable state of Tc produced by the KMS-2 is the origin of the decrease in Tc D_{obs}. From this result, sulfide-containing materials should be further investigated to help improve Cast Stone performance (or any other cementitious material).

1. Introduction

One of the greatest challenges facing the world today is the development of a secure, low-carbon energy supply. Nuclear power a well-developed technology with a potential to play a key role in such development. Public discussion about nuclear power has focused on the long-term management and disposal of radioactive waste, a by-product from energy and weapons production, the majority of which is currently kept in temporary storage although some low level waste repositories are in operation around the globe. Thus, the future development of nuclear power is critically dependent on bringing closure to the fuel cycle, with the assurance of safe, long-term storage of used fuel and all resulting nuclear waste, including legacy waste. Liquid nuclear wastes are generated from processing of used nuclear material and are currently included in the nuclear inventory of several countries including the United States, Japan, France, the United Kingdom, Canada [1], and Germany [2]. Vitrification to produce a borosilicate glass (or alumino-phosphate glass in Russia) [3] is the baseline technology for immobilization of radioactive liquid wastes, owing to the long-term chemical stability of glass. However, vitrification requires high temperatures (> 1000 °C) and certain radionuclides, including technetium-99 (Tc) [4] and iodine-129 (I), [5] are highly volatile at such temperatures. The result is limited incorporation of the volatile radionuclides into the final waste form and generation of secondary waste streams that require additional immobilization and management.

The challenge of immobilization of liquid nuclear wastes containing volatile radionuclides is best exemplified by the environmental clean-up mission currently ongoing at the U.S.A. Department of Energy (DOE) Hanford site, located in southeastern Washington, U.S.A. Nine reactors at the Hanford site produced 67 tons of plutonium from 1943-1989 [6]. As a result of the Pu production, a large inventory of radioactive wastes with widely different compositions were generated. Fifty-six million gallons of the waste currently remain stored in 177 storage tanks at the site [7]. Initially, waste tanks were comprised of a single carbon steel shell, which began to leak in 1959 due to the corrosive nature of the wastes [8]. In total, 67 of the 149 single shell tanks have leaked and the drainable and pumpable liquid waste has now been transferred to more robust double shell tanks. However, the double shell tanks themselves are now approaching the end of their design life and the first leak from a primary tank into the secondary liner of a double-shell tank has recently been discovered [9]. Thus, it is imperative that these wastes be removed from the tanks and immobilized in a timely manner.

Current management plans of the Hanford tank wastes calls for separated into high-level (high radioactivity and low volume, HLW) and low-activity (high radioactivity and lower volume , LAW) waste streams. The waste streams will be vitrified at the Hanford Tank Waste Treatment and Immobilization Plant (WTP). Much of the technetium is expected to volatilize out of the molten glass and become trapped in the gas scrubber. Given the volume of LAW to be treated at WTP, and the generation of secondary waste streams, including the aqueous solution from the gas scrubber, alternate solidification technologies are being investigated to assist in the clean-up mission. Cementitious waste forms present suitable characteristics for treating Tc

containing wastes as their fabrication temperatures are below the volatility point of Tc and their low fabrication costs are favorable for immobilizing large volumes of waste. Cementitious waste forms are currently used for the immobilization of liquid wastes at the DOE Savannah River site, [10,11] at other global waste treatment sites for low level wastes,[12] and under consideration as an immobilization technology in several countries [13,14]. The most prominent issue influencing the use of cementitious waste form technologies is the ability to demonstrate that the retention of radionuclides of concern, such as Tc, is sufficient to ensure insignificant environmental impact from the waste disposal.

The environmental risk associated with Tc release from immobilized waste forms is high due to the long half-life of Tc (213,000 years) and its high mobility in subsurface environments. In oxidizing environments, Tc primarily exists in an oxyanion form, pertechnetate (TcO_4^-). TcO_4^- has limited adsorption onto many common minerals including silicates, carbonates and sulfates (e.g. biotite, apatite, dolomite and gypsum) from the aqueous phase [15,16]. As a result, TcO_4^- in groundwater will migrate rapidly under oxic conditions, irrespective of the biogeochemistry, climate, and physical characteristics of the site [17,18]. At the Hanford site, a significant Tc plume exists in the subsurface [19] resulting from the tank leaks. Given this unhindered migration through the subsurface, any release of Tc from a waste form must be kept to a minimum.

At the Hanford site, both glass and cementitious waste will be stored at the Integrated Disposal Facility (IDF). The IDF is a landfill design which measures 457 m × 233 m × 13 m (from the surface) and was constructed in 2006, although has not accepted any waste to date. The projected volume of immobilized LAW to be generated exceeds the current expected capacity of the vitrification facilities. To overcome this limitation, Cast Stone, a cementitious waste form comprised of a dry mix of 47 wt% blast furnace slag, 45 wt% fly ash and 8 wt% ordinary Portland cement, is currently being considered as a possible candidate waste form to provide additional LAW immobilization capacity [20,21].

Investigations to determine the optimum dry to wet mix ratio of Cast Stone with various LAW simulants, containing a combination of Tc, I, and U spikes, were conducted previously using EPA Method 1315 leach testing [22,23]. The EPA Method 1315 test involves placing a monolithic sample into a leachant at a surface area to volume ratio of 1 cm^2 : 9 mL for a set interval duration, after which the monolith is removed and placed into fresh leachant and repeated [23]. From these investigations, it was determined that Cast Stone had promising properties for retention of Tc, although release was influenced by variations in the Cast Stone composition [20]. It was concluded that retention of radionuclides by the Cast Stone, and cementitious waste forms in general, may be improved through the inclusion of materials which can selectively sequester radionuclides or contaminants of interest in both the liquid state and final waste form, termed getters [24].

A range of getter materials that target and sequester Tc from aqueous media has been investigated in the scope of nuclear research, including metal oxides [25], nanomaterials [26,27],

carbon-based materials [28], aluminophosphates [29], and resins [30,31]. Many of these materials showed promise for the removal of Tc from chemically inert aqueous environments at circumneutral pH and with low ionic strengths [32-34]. However, a drastic drop in performance was observed with many Tc getters upon moving to extreme chemical environments with high ionic strength, high/low pH and presence of competitive redox-active species. These more extreme conditions are relevant to removal of Tc from LAW because it has a high pH (> 13), high ionic strength (between 5 M and 8 M Na), and contains high levels of redox-active species, such as Cr(VI) and NO_3^-. Two getter materials have recently shown high promise for the removal of Tc from chemically complex environments, including LAW: Sn(II)-treated apatite (Sn-A)[35] and layered potassium metal sulfide (KMS-2)[36]. Although the mechanisms vary, both the Sn-A and KMS-2 sequester Tc from solution through reduction of Tc(VII) to Tc(IV). The Sn-A sequesters Tc as a Tc(IV)-oxide and KMS-2 as a Tc(IV)-sulfide. These Tc(IV) species have far lower solubility than Tc(VII) species, which decreases Tc mobility.

Both Sn-A and KMS-2 are suitable candidates to be used as Tc getters incorporated into Cast Stone or other cementitious waste forms based on previous testing. Here, we present for the first time the process of fabrication, followed by rigorous testing and thorough characterization of the Cast Stone waste form containing either Sn-A or KMS-2 as a Tc getter for solidification of a representative chemically extreme (i.e., high pH and ionic strength) LAW simulant. By using the two getters, a comparison between the stability of two forms of Tc(IV) can be made upon introduction to a cementitious waste form. EPA method 1315 leach testing was conducted using simulated Hanford vadose zone pore water, which is the likely contacting solution for a waste form placed at the IDF. Advanced solid phase characterization techniques including x-ray absorption spectroscopy (XAS), micro-x-ray fluorescence (μ-XRF), and novel single-particle digital autoradiography (iQid) were used. These techniques, in combination with the results from the XRD analyses and leachate concentrations, provide insights into Tc molecular associations in Cast Stone and aid in the understanding of mechanisms and pathways that control Tc release from getter-containing Cast Stone.

2. Experimental Details

2.1 Solution Preparation

2.1.1 Low Activity Waste Simulant

The Cast Stone samples in this study were prepared using a LAW simulant with an average target Na content of 6.5 M. This LAW simulant is based on the Hanford Tank Waste Operations Simulator (HTWOS) model, which supports the River Protection Project System Plan Revision 6 [37]. The composition of the LAW simulant is given in Table 1. Distilled deionized water (DDI, 18.2 MΩ·cm) was used and the chemicals (Sigma-Aldrich or Fisher Scientific) were added in the order given in Table 1. Each chemical was added individually while the simulant was being stirred; the compound was allowed to fully dissolver prior to adding the next one.. If

required, the simulant was heated to ~ 70 °C to facilitate chemical dissolution. After the addition of the final chemical, the simulant was stirred and cooled for ~ 16 h before DDI was added to reach the target mass. The measured composition of the LAW simulant after fabrication is also listed in Table 1. The long term leached Cast Stone sample presented in this work was fabricated with a similar LAW simulant with a Na concentration of 8.3 M.

Table 1 - Composition of the LAW Simulant utilized in Cast Stone formation.

Compound	Amount for 1 L (g)	Anion/Cation	Measured Concentration (g/L)	Concentration (mol/mol Na)
DDI	200 mL	**Na**	153.33	1.000
KNO_3	4.60	**Al**	11.75	0.065
NaCl	3.04	**Cl**	3.47	0.015
NaF	1.64	**NO_3**	140.00	0.339
Na_2SO_4	15.70	**NO_2**	37.04	0.121
$Al(NO_3)_3•9H_2O$	148.74	**SO_4**	11.58	0.018
NaOH (50% soln)	289.12	**K**	2.08	0.008
$Na_3PO_4•12H_2O$	24.71	**PO_4**	1.47	0.002
$NaC_2H_3O_2$	6.64	**Free OH**	35.39	0.312
Na_2CO_3	37.89			
DDI	100 mL			
$Na_2Cr_2O_7•2H_2O$	2.31			
DDI	100 mL			
$NaNO_3$	74.03			
$NaNO_2$	50.68			
DDI	100 mL			

The LAW simulant was spiked with Tc using a 10 400 ppm $NaTcO_4$ stock solution to a target spike of 16 ppm, and with I using a 10 000 ppm NaI stock solution to a target spike of 5 ppm (only the results for Tc will be described in this paper). The HTWOS model predicts a Tc concentration of 4.6 ppm for a 6.5 M Na concentration, thus the 16 ppm spike level is ~ 3.5 times the predicted HTWOS value and allows for comparison to previous Cast Stone tests using a similar Tc content. The long-term leached Cast Stone samples analyzed in this report were spiked with 56 ppm Tc (10 × the Tc concentration predicted by HTWOS for a LAW simulant with a Na concentration of 7.8 M) to aid in ability to detect Tc in solid state analytics.

2.1.2 Hanford Vadose Zone Porewater

The simulated Hanford vadose zone pore water (VZPW) used for leach testing (Table 2) was developed based on several measurements of actual VZPW removed from a borehole of Hanford formation sediments where the IDF is located [38]. A large field sample of moist sediment was removed from Hanford formation sediments using cable tool drive barreling. The field moist sediments were then ultra-centrifuged for several hours. Small volumes of solution were passed through the sediment and collected. When approximately 30 to 50 mL of solution was collected from each sediment sample it was immediately filtered through 0.45 μm membrane filters and analyzed for chemical composition. The results from characterizing the pore water from two depths (48.5 and 82.5 feet below ground surface) from a borehole from the IDF location (specifically borehole C4124; 299-E27-22) [38] were averaged and charge balanced. Reagents were added, in the order given in Table 2, to the corresponding volume of distilled water.

Table 2 - Composition of the simulated Hanford vadose zone pore water (VZPW) used in EPA Method 1315 leach testing.

VZPW Recipe			
Order	**Molarity (mol/L)**	**Reagents**	**g/L**
1	0.012	$CaSO_4 \bullet 2H_2O$	2.07
2	0.0017	NaCl	0.10
3	0.0004	$NaHCO_3$	0.03
4	0.0034	$NaNO_3$	0.29
5	0.0026	$MgSO_4$	0.31
6	0.0024	$MgCl_2 \bullet 6H_2O$	0.49
7	0.0007	KCl	0.05
Adjust pH to 7.0 (±0.2) with sodium hydroxide or sulfuric acid dependent on initial pH.			

2.2 Cast Stone Fabrication

2.2.1 Selection of Tc Getters

Two Tc getters were selected for Cast Stone fabrication based on previous work. Sn(II)-treated apatite (Sn-A), fabricated as described in Asmussen et al. [35], was selected based on its ability to reduce Tc(VII) to Tc(IV) and produce a $Tc(IV)O_2 \cdot x\ H_2O$ final product [35]. The likely chemical formula is $Ca_{x-y}Sn_y(PO_4)_x(X)$, where X is the supporting anion being either OH, F or Cl. The Sn-A used in this study has a reduction capacity of 3469 ± 530 microequivalents (μeq) of electrons/g[35] measured using the Ce(IV) reduction capacity method [39]. Sn-A has shown preferential reduction of Cr(VI) over Tc(VII) and is deleteriously affected by high alkaline environments [35]. To assure maximum aqueous Tc removal, the mass of added Sn-A (i.e., 50 g) was theoretically capable of reducing ~ 3 times the Cr(VI) content and 10 times the Tc content of the LAW simulant.

Potassium metal sulfide (KMS-2) was developed as a material for removing hazardous cationic species from different solutions[40,41]. KMS-2 has also shown the highest performance of Tc(VII), as TcO_4^-, removal from LAW [36]. The KMS-2 used in this report was fabricated using the solid state approach described in Neeway et al. (2016) [36] and has a composition of $K_{1.3}Mg_{0.95}Sn_{2.1}S_6$ [40]. The sulfide component of the KMS-2 structure provides a reduction capacity of 21 000 μeq electrons/g [36] and produces a final Tc product of $Tc(IV)_2S_7$ With this high reduction capacity and ability to function as an excellent Tc getter under high alkaline conditions, 2.35 g of the KMS-2 was added, which is enough to theoretically reduce all of the Cr(VI) and 10 times the Tc content present in the LAW simulant.

Silver exchanged zeolite (Sigma Aldrich) was also added to all systems to act as an iodide getter, the results of which are not presented in this work.

2.2.2 Cast Stone Fabrication

The compositions for the Cast Stone samples in this study are provided in Table 3. The Cast Stone has a composition of 47 wt% blast furnace slag (BFS), 45 wt% fly ash (FA) and 8 wt% ordinary Portland cement (OPC). The Cast Stone was fabricated with a free water to dry blend ratio of 0.55. The mass of getter added was subtracted from the mass of the required dry materials. The remaining mass was comprised of the 47:45:8 BFS:FA:OPC ratio and the BFS, FA and OPC combined thoroughly prior to fabrication.

Table 3 – Fabrication recipes for the Cast Stone samples used in this study.

Batch ID	Total Dry Ingredients (g)	LAW[(1)] Simulant Required (g) [(2)]	Tc Spike (ppm)	Blast Furnace Slag (g)	Fly Ash, (g)	OPC (g)	Mass of Tc Getter (g)	Mass of I getter (g)
CS-Control	1750.0	1307.9	16	822.5	787.5	140.0	n/a	n/a
CS-Sn-A	1750.0	1307.9	16	798.3	764.3	135.9	Sn-A 50.0	Ag-Z 8.75
CS-KMS-2	1750.0	1307.9	16	820.7	785.8	139.7	KMS-2-SS 2.35	Ag-Z 1.45
Long Term Cast Stone	1767.5	1302.7	56	822.5	787.5	140.0	Sn-A 8.75	Ag-Z 8.75

The getter was added to the liquid LAW simulant and allowed to react before the addition of the dry Cast Stone ingredients. The Sn-A was allowed to react for 48 h and the KMS-2 was allowed to react for 24 h with the LAW simulant. The shorter reaction time for KMS-2 is

because, based on previous observations, Tc removal by the KMS-2 is faster than Sn-A [34]. Aliquots of the liquid LAW simulant were collected before and after getter addition to determine the extent of Tc removal by the getters.

Following the getter treatment the LAW simulant was stirred thoroughly using an electric mixing impeller to ensure that the getter material was well dispersed. The dry Cast Stone components were then introduced slowly over a 5 min time span with continual mixing. The impeller rotation rate was kept at a level to ensure that little to no vortex was created to limit air introduction to the mix. From the initial time of dry component addition, the mixture was allowed to stir for 15 min. The Cast Stone was then poured into cylindrical plastic molds (2" diameter × 4" height) and vortexed to remove any entrapped air. The molds were capped with a perforated lid, placed into a sealed bucket and allowed to cure for 28 d at 100 % relative humidity. This fabrication produced three sample sets: 1) a control sample with no getters added (CS-control), 2) the Sn-A containing Cast Stone (CS-Sn-A) and 3) the KMS-2 containing Cast Stone (CS-KMS-2).

2.3 EPA Method 1315 Leach Testing

Full details of Method 1315 leach testing are provided by the EPA[23], and a summary is given here. After curing, the monoliths were weighed and placed in a holder consisting of a plastic top ring and a 2" diameter plastic pipe bottom held together with fishing line. This holder design ensures no more than 2 % of the overall surface of the monolith was covered by the holder. The monoliths were placed into 2 L plastic buckets containing VZPW at a 9 mL : 1 cm^2 surface area ratio (~1700 mL VZPW). The buckets were capped but air was not removed from the headspace (i.e., leaching occurred under atmospheric conditions and in the presence of atmospheric O_2 and CO_2). At the conclusion of each leaching interval, the monoliths were removed from the VZPW, weighed, photographed and then placed into other buckets filled with the appropriate amount of fresh VZPW leachant. The leaching intervals were 2 h, 1 d, 2 d, 7 d, 14 d, 28 d, 42 d and 63 d. The leachates were analyzed with inductively coupled plasma mass spectroscopy (ICP-MS) for Tc or inductively coupled plasma optical emission spectroscopy (ICP-OES) for Cr and Na. Ion chromatography (IC) was utilized for anion measurements, e.g., NO_3^-.

2.4 Spectroscopy

2.4.1 X-ray diffraction (XRD)

XRD was used to determine the mineralogical composition of the samples. Powdered samples were loaded into zero-background holders and diffraction data were collected with a Rigaku Miniflex II Bragg-Brentano diffractometer using Cu-Kα radiation (λ = 1.5418 Å) and a graphite post-diffraction monochromator. A known amount of rutile (TiO_2) standard was added to each sample for quantitative analysis. Quantitative Rietveld refinements were carried out with the Bruker TOPAS software (v4.2, Bruker AXS) using crystal structures for the relevant phases.

252

253 *2.4.2 Single Particle Digital Autoradiography (iQid)*

254 "Single-particle digital autoradiography", with the ionizing-radiation Quantum Imaging
255 Detector (iQID) [42], was used to assess the spatial distribution of ^{99}Tc within cross sectioned Cast
256 Stone "pucks". The iQID imager comprises a scintillator (ZnS) in direct contact with a micro-
257 channel plate image intensifier and a lens for imaging the intensifier screen onto a charge
258 coupled device (CCD) or complementary metal oxide semiconductor (CMOS) camera sensor, all
259 within a compact light-tight enclosure. Individual photons or particles absorbed in a scintillator
260 crystal or phosphor screen produce a flash of light that is amplified via the image intensifier by a
261 factor of 10^4 to10^6 and then imaged onto the camera. Scintillation flashes associated with
262 individual events are captured with high resolution with an array of pixels and referred to as an
263 event cluster. iQID's ability to localize charged particles, both spatially and temporally, on an
264 event-by-event basis enables radionuclide distributions to be quantified at mBq-levels.
265 Autoradiographs are constructed in real time at high spatial resolution with an unrestricted
266 dynamic range. For the Cast Stone cross section imaging experiments, a 4-megapixel camera
267 (2048 × 2048 pixels) was used that acquires full-resolution images at approximately 10 frames
268 per second. Disks sectioned from within ~ 0.5" of the center of the Cast Stone monoliths were
269 analyzed using the iQID. The disks, which had a smooth surface, were placed on a scintillation
270 screen for collection times of 45 h. The effective physical size of each pixel during the image
271 acquisition was 55.8 μm with the final images displayed having an effective pixel size of 111.5
272 μm (2x2 binning). The pixel value corresponds to the number of beta particles detected at that
273 location during the 45 h image run. A test sample with small droplets of TcO_4^- enclosed in mylar
274 film was also analyzed to ensure the β-decay signal arises from specific sample areas, with a
275 strong correlation. Further information regarding development and use of the technique can be
276 found in Miller et al. [42].

277 *2.4.3 X-ray Absorption Spectroscopy (XAS)*

278 Tc K-edge X-ray absorption spectroscopy (XAS) data were obtained at the Stanford
279 Synchrotron Radiation Lightsource Beamline 11-2. The monochromator was detuned 50% to
280 reduce the harmonic content of the beam. Transmission data was obtained using Ar-filled ion
281 chambers. Fluorescence data were obtained using a 100 element Ge detector and data were
282 corrected for detector dead time. Raw XAS data were converted to spectra using SixPack [43].
283 Spectra were normalized using Athena[44]. Non-linear least squares fits of the normalized X-ray
284 absorption near edge spectroscopy (XANES) spectra were obtained using standard spectra and
285 the locally-written program, *fites* (http://lise.lbl.gov/RSXAP). XANES standard spectra were
286 carefully energy calibrated using TcO_4^- adsorbed on Reillex-HPQ as the energy reference. The
287 XANES spectral resolution is 7 eV based on the width of the TcO_4^- pre-edge peak. Sample
288 spectra were convolved with a 1.8 eV Gaussian to match the resolution of the TcO_4^- adsorbed on
289 Reillex-HPQ standard spectra. Six standard spectra (TcO_4^-, Tc_2S_7, Tc(V)=O polyoxometallate,

Tc(IV) gluconate, $TcO_2 \cdot 2H_2O$ and a Tc(IV) EDTA complex) were used in the initial fitting of the sample XANES spectra. Cast Stone samples were selected and ground with a mortar and pestle to < 300 μm particle size for XAS analyses.

2.4.4 Micro X-ray Fluorescence Spectroscopy (μ-XRF)

μ-XRF provides elemental distribution information within a sample. μ-XRF analysis was performed on un-leached Cast Stone samples using an Orbis Micro-XRF Analyzer with a Mo X-ray source and a silicon drift detector. Elemental data were collected under vacuum using a 45 kV polychromatic beam focused to 30 μm using a poly-capillary optic and displayed as number of counts per element-specific energy levels. The Cast Stone samples used for μ-XRF were chiseled from the Cast Stone pucks used in iQid imaging. The samples were mounted in epoxy resin (Streuers) in a stainless steel ring. After mounting, the sample was sliced using a low speed disc saw (Isomet) to a thickness of ~ 100 μm. The sample was then polished, water free, to a 0.1 μm diamond finish. The thin slide sample was then analyzed with iQid and μ-XRF.

3. Results and Discussion

3.1 Tc Removal by Getters

In order to limit diffusivity from the Cast Stone into the leachant, the Tc must first be removed from the LAW simulant solution by the getters. Figure 1 a) shows the percentage of initial Tc (16 ppm) removed from the LAW simulant by the getters. Sn-A added at a 50 g : 1 L ratio removed 65% of the Tc from solution, below the theoretical removal capacity. This is within the range of removal previously observed at this ratio of Sn-A to Tc [35]. The expected product of the removal is $Tc(IV)O_2 \cdot xH_2O$. The KMS-2 removed 98 % of Tc from the LAW with a ratio of only 2.35 g : 1 L. The final product of the Tc removal from LAW has been identified as a $Tc(IV)_2S_7$ species [36], comprised of two Tc centers connected through a sulfide linkage [45]. This minimal amount of KMS-2 added to achieve high levels of Tc removal highlights the prospect of sulfide-bearing materials to be used for redox treatments under chemically extreme conditions.

The results show that not all of the Tc(VII) initially in the LAW simulant was removed by the getter, even though a sufficient mass of each getter was added to provide a reduction capacity capable of complete Tc removal. One reason why not all of the Tc(VII) was removed is that Cr(VI) in solution can hinder Tc(VII) removal by getter materials through competitive redox processes. Cr(VI) has a higher standard reduction potential of 1.33 V compared with 0.78 V for $Tc(VII)O_4^-$ [46,47] and thus Cr(IV) is preferentially reduced. Figure 1 b) shows the % Cr removed by the getters prior to fabricating the LAW simulant. The Sn-A removed > 99% of the initial Cr, 873 ppm, from the LAW simulant. Following contact with the Sn-A, the LAW simulant lost its yellow color and became colorless, indicating reduction and subsequent removal of the Cr(VI). This level of Cr removal by the Sn-A suggests that it could be utilized for the removal of Cr(VI)

and other competitive redox species, with subsequent addition of a second material to target any remaining redox active species.

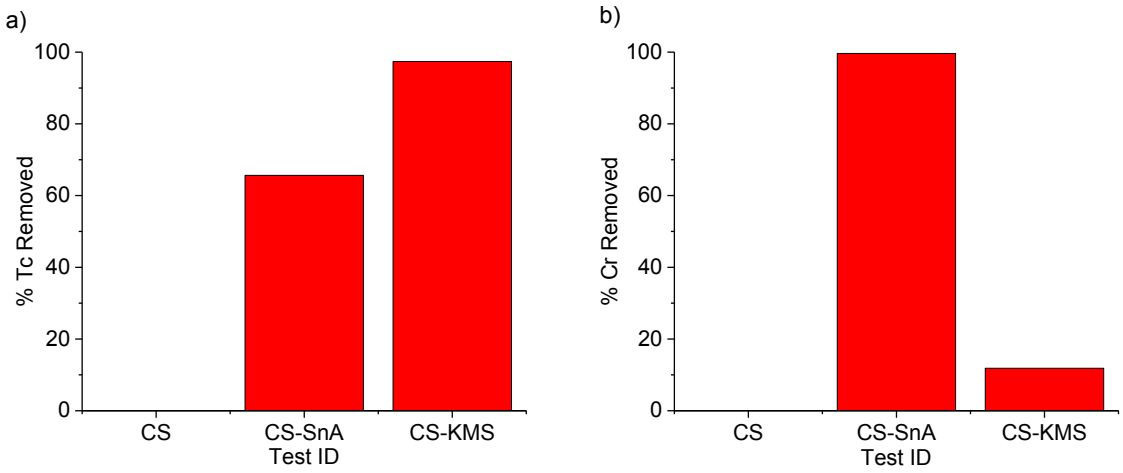

Figure 1 - the percentage of initial concentration of a) Tc (16 ppm) and b) Cr (873 ppm) removed from the LAW simulant by the Tc getters prior to Cast Stone fabrication.

On the other hand, KMS-2 only removed 12 % of the Cr from the LAW simulant. Given the high reductive capacity of KMS-2, it is likely the Cr(VI) was reduced, in a similar way to the case when Sn-A was used. Although, a color change in the LAW simulant from yellow to green-blue after contact with the KMS-2 was observed, which suggests Cr(VI) reduction to Cr(III), it appears that reduced Cr(III) was not removed from solutions and is likely present as a soluble Cr(III) species. In both the Sn-A and KMS-2 cases, the amount of Tc getter added was based on: (i) the reductive capacity of the material; and (ii) overcoming deleterious effects of pH and competing redox reactions on getter performance. The results from our study demonstrated that this approach led to highly successful Tc removal from the LAW simulant, and should be used in future efforts of this and similar types.

3.2 Leach Testing of Getter-Containing Cast Stone

3.2.1 Measurement of Observed Diffusivity

Cementitious waste forms are comprised of a complex, porous structural matrix. As a result, diffusion of species out of the matrix via physical processes is restricted[48]. The chemical reactivity of the cementitious waste form also adds additional restraints to diffusion of species from the waste form to the contacting solution; more so in the presence of chemically reactive getters. Therefore, the release of species from cementitious materials is best represented if both chemical reactions and physical processes are considered [49,50]. Although operationally defined, the observed diffusivity (D_{obs}) incorporates the effects of both factors and is most suitable for

measurement and comparison of diffusion (i.e., release) rates of contaminants of interest from a cementitious waste form.

Observed diffusivity is calculated for individual species using a solution for Fick's 2nd law for simple radial diffusion into an infinite bath from a cylinder shape, similar to the one used in Cast Stone leaching through EPA Method 1315. The effective diffusivity is calculated after each leaching interval using Equation 1:

$$D_{obs} = \pi \left[\frac{M_{t_i}}{2\rho C_o(\sqrt{t_i} - \sqrt{t_{i-1}})} \right]^2 \quad \text{Equation 1}$$

where D_{obs}= observed diffusivity of a specific constituent for leaching interval, *i* (m^2/s)

M_{ti} = mass of specific constituent released during leaching interval (mg/m^2)

t_i = cumulative contact time at the end current leach interval, *i* (s)

t_{i-1} = cumulative contact time after previous leaching interval, *i-1* (s)

C_o = initial concentration of constituent relative to the dry Cast Stone mass (mg/kg_{dry}) calculated using the theoretical initial constituent concentration in the simulant based on additions made in simulant preparation.

ρ = Cast Stone dry bulk density (kg_{dry}/m^3).

The common units for observed diffusivity are cm^2/s and the output from equation 1 (m^2/s) is multiplied by 10 000 to convert to these units.

The D_{obs} term is also defined from the quotient of an intrinsic diffusivity (D_i) and a chemical capacity factor (α). This relationship is shown in equation 2:

$$D_{obs} = \frac{D_i}{\alpha} \quad \text{Equation 2}$$

The D_i term is representative of the physical influence impacting diffusion from the cementitious material. The value of D_i depends on the tortuosity (τ), constrictivity (δ) and porosity (ε) of complex cementitious structure. These factors adjust the diffusion coefficient of a solute in dilute water (D_f) in equation 3.

$$D_i = D_f \frac{\varepsilon\delta}{\tau^2} \quad \text{Equation 3}$$

The tortuosity term is representative of the diffusing species traveling a longer distance than assumed in a linear diffusion pathway due to the porous network within the cementitious waste form. The constrictivity term depends on the ratio of the diameters of the smallest and

largest pores in the system. Both are dimensionless parameters and, along with porosity, are dominantly used in models as empirical parameters to measure D_{obs}.

The chemical component, α, is utilized to combine a myriad of interactions between species and the cementitious material including redox processes, ion exchange, sorption and associated kinetics. Assuming fast and reversible chemical interactions and sorption processes that follow a linear isotherm, α can be calculated as follows:

$$\alpha = \varepsilon + \rho K_d \quad \text{Equation 4}$$

Where K_d is the distribution coefficient representing the ratio of the amount of a species sorbed to a solid surface vs. the amount present in solution at equilibrium. For species that do not interact with the waste form, such as Na^+ and NO_3^-, a K_d of zero would be expected and the value of the chemical component α would depend solely on the porosity. Such species are termed to be "mobile". In the case of redox sensitive species, the K_d and the chemical component α will be influenced by sorption and redox reactions, and a comparison between the D_{obs} value measured for the redox sensitive species and a mobile constituent should be performed to determine the effect of the additional chemical reactions on contaminant diffusivity.

3.2.2 EPA Method 1315 Leach Testing

Following the 28 d curing procedure, the Cast Stone monolith samples were leached in simulated Hanford VZPW using the conditions described in EPA Method 1315. VZPW represents the likely disposal conditions experienced by a waste form in a shallow subsurface disposal site, such as the IDF. The Tc D_{obs} over a 63 d leaching time for the three Cast Stone systems is shown in Figure 2 a). The control monoliths without Tc getters added (CS-Control) showed a continual increase in Tc D_{obs} before reaching a steady state at 42 d. After 63 d leaching, the Tc D_{obs} for the CS-Control was $4.6 \pm 0.2 \times 10^{-12}$ cm^2/s. This value is within the expected range of previous measurements of Cast Stone fabricated with simulated LAW [51]. In the most recent *Tank Closure and Waste Management Environmental Impact Statement for the Hanford Site, Richland, Washington*[52], the Washington State Department of Ecology highlights that lowering the diffusivity of a species to a performance standard of 1×10^{-12} cm^2/s at a groundwater infiltration rate of 3.5 mm/y would "delete this waste (i.e. the waste form being investigated) from the list of dominant contributors to risk".

As the Tc getters act by reducing the $Tc(VII)O_4^-$ to an sparingly soluble Tc(IV) species, a chemical oxidation step is required in order for the Tc to be released. This is highlighted by measurement of the D_{obs} for a "mobile constituent" which does not chemically interact with the Cast Stone. Figure 2 b) displays the Na D_{obs} measured during the leaching period. It should be noted that the baseline Na content (5 mmol/L)of the VZPW was subtracted in the calculation of D_{obs}. For the CS-Control, the Na D_{obs} continually decreased from $1.7 \pm 0.6 \times 10^{-8}$ cm^2/s at the 1 d interval to $3.9 \pm 0.1 \times 10^{-9}$ cm^2/s at the 63 d interval. The Tc D_{obs} values are many orders of

magnitude lower than the "mobile" Na D_{obs} value, indicating that the mechanism of Tc release is a slow chemical reaction involving re-oxidation of the Tc. In the CS-Control, a portion of the Tc will be present in a reduced Tc(IV) state due to the reducing BFS component within the Cast Stone[45].

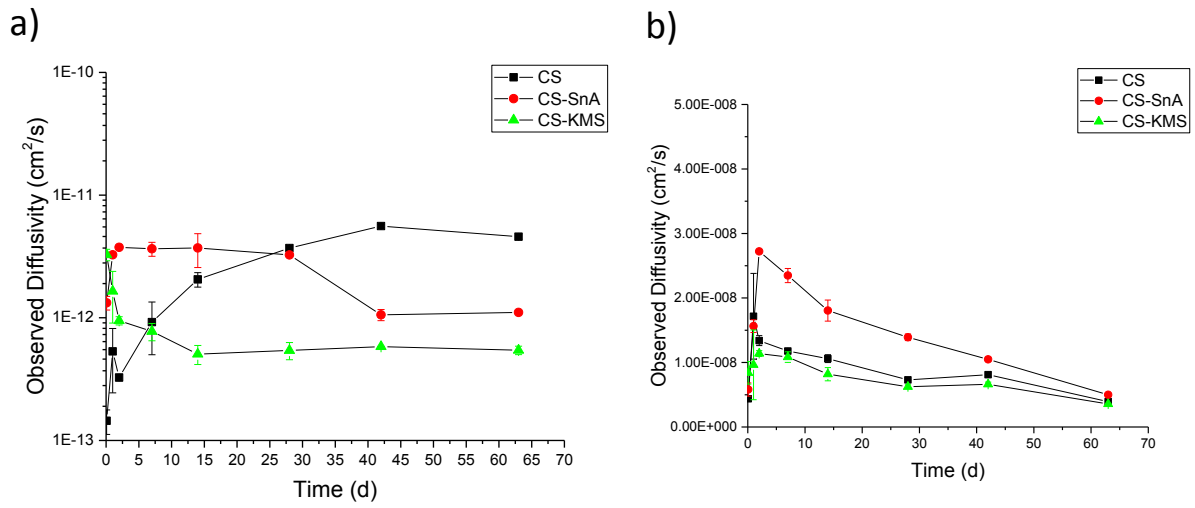

Figure 2 - a) the resulting Tc D_{obs} measured and b) the resulting Na D_{obs} values during the 63 d leaching period of the Cast Stone monoliths with and without Tc getters. The Cast Stone monoliths were leached in VZPW and placed into a fresh leachant at each interval at a sample surface area to leachate volume of 1 cm^2 : 9 mL. The errors bars represent the standard deviation of the mean on the two leaching samples.

The D_{obs} values measured for Tc leached from the Cast Stone samples containing Sn-A (CS-Sn-A) during the first 28 d interval are higher or equal to the CS-Control (Figure 2a). After 28 d, the Tc D_{obs} values decreased to $1.1 \pm 0.01 \times 10^{-12}$ cm^2/s at 63 d. In longer leaching times, the presence of the Sn-A getter improved the retention of Tc. It is possible that the Sn-A may have increased the release of species from the Cast Stone monolith. In the Na D_{obs}, (Figure 2 b), the CS-Sn-A also had the highest measured values in the initial stages of leaching reaching a maximum of $2.7 \pm 0.002 \times 10^{-8}$ cm^2/s at the 2-d interval. As no interactions occur between Na and the Cast Stone, this increase must arise from the physical properties of the monolith, as described previously. The CS-Sn-A included 50 g of Sn-A added in the Cast Stone, and this large addition of material may have distorted the structure, leading to larger pore sizes and allowing for more rapid diffusion of species. This highlights the need to consider physical impacts resulting from addition of getters to cementitious materials.

The KMS-2 was highly successful in sequestering Tc from the LAW simulant prior to fabrication of the Cast Stone. By removing > 98 % of the Tc from solution, this system provided the greatest Tc retention in the Cast Stone. The Tc D_{obs} values measured for the KMS-2 containing Cast Stone (CS-KMS-2) in Figure 2 a) support this hypothesis. The Tc D_{obs} for the CS-KMS-2 monolith after 2 d were below the D_{obs} for the CS-Control, with little change over

time. At 63 d, the Tc D_{obs} was $5.4 \pm 0.4 \times 10^{-13}$ cm^2/s, a near order-of-magnitude improvement over the CS-Control. This substantial improvement was achieved with only a minor addition of KMS-2, equivalent to < 0.01 wt% of the overall mass of the waste form. KMS-2 as a Tc getter is highly effective in removing Tc from extreme chemical environments and controlling Tc release from the subsequently fabricated Cast Stone waste form. The Na D_{obs} for the CS-KMS-2 system was similar to the CS-Control ($3.6 \pm 0.7 \times 10^{9}$ cm^2/s at 63 d leaching). Further studies to determine the ideal KMS-2 getter loading amount and investigate the performance of other sulfide-containing materials as Tc getters are ongoing.

3.3 Characterization of Tc Getter Containing Cast Stone

3.3.1 Cast Stone Characteristics

Solid-phase characterization of the monolith samples provides information on the mechanism of Tc location and retention in the Cast Stone. Although the Cast Stone samples are relatively similar in mineralogical composition throughout, see Supplemental Information Table S1, visible differences exist between the Cast Stone samples, as shown in the photographs Figure 3. Following curing, the interior and exterior of the CS-Control and the CS-KMS-2 look identical, Figures 3 a) and c), respectively. Both samples display a dark blue-green interior as a result of the presence of sulfur based radicals from the blast furnace slag. As is typical of blast furnace slag based cement, the dark blue color fades to gray upon oxidation. However, after 63 d leaching in VZPW, two primary features developed on the exterior of the CS-Control and CS-KMS-2. First, a white film forms on the monolith wall, beginning at the 1 d interval. This white deposit was identified by XRD as aragonite (a $CaCO_3$ polymorph). Growth of this film may contribute to the slowed release of species from the Cast Stone to solution over long exposure timeframes by providing a physical barrier to diffusion. However, after 63 d leaching, this film is not uniform, nor complete. Dark regions, denoted by white arrows in Figures 3 a) and b), also developed during the leaching period and these regions were further investigated using scanning electron microscopy. Tc was only identified within this dark region and not outside of it (see Figure S1 in the supplemental information).

The CS-Sn-A (Figure 3 c) displayed increased heterogeneity compared with the CS-Control. A blotchy pattern can be seen on the exterior of the monolith, likely a result of the higher loading of the getter added to the Cast Stone. Another observation was made upon opening the monolith: the dark blue-green color was present in the interior regions of the monoliths and two additional features were also prominent. These are white, isolated regions (marked with an arrow in the figure), which are surrounded by a region of brown coloration. Samples from both white and brown areas were collected and analyzed by XRD. The white areas were primarily comprised of burtite ($CaSn(OH)_6$) and cassiterite (SnO_2), and are both remnants of the added Sn-A. The brown region surrounding the white areas was similar to the bulk Cast Stone (i.e., highly amorphous), but also contained burtite. This heterogeneity confirms that the distribution of getters within the Cast Stone matrix is uneven.

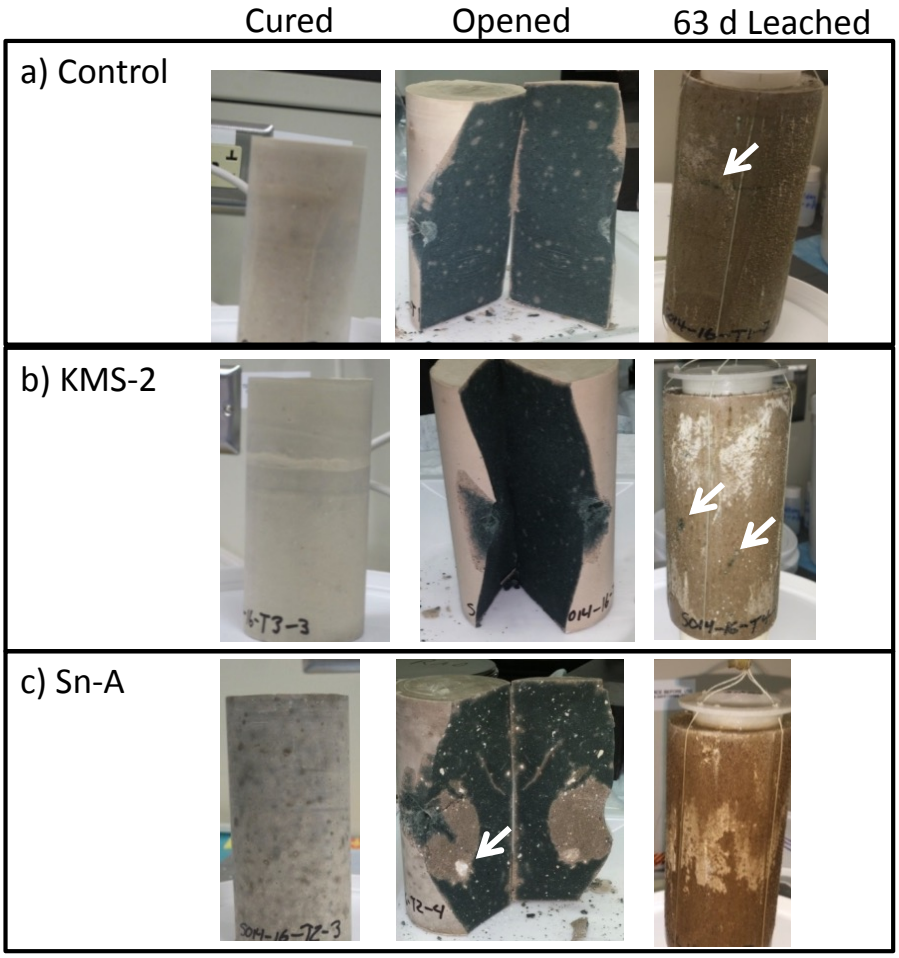

Figure 3 - photographs of the Cast Stone monoliths in their cured form, opened after curing and following 63 d leaching for a) the control system with no getters, b) Sn-A containing Cast Stone and c) KMS-2 containing Cast Stone

3.3.2 Tc Distribution in Cast Stone

To develop an understanding of Tc behavior in Cast Stone, the Tc must be located within the sample and the chemical composition of these locations characterized. With the low overall concentration of Tc in the leached samples (16 ppm in the LAW simulant, or 5 µg Tc/kg of wet Cast Stone), Tc cannot be detected through the use of many conventional spectroscopic techniques. However, Tc does possess a unique signature in its β-decay which can be utilized to map its distribution within the Cast Stone.

Traditional contact radiography has been previously utilized to image Cs and Sr distribution in cementitious materials[53]. The drawback of this technique is it is an "all in" measurement in that the analyst must wait until the end of the measurement to observe if a useful image has been produced on the radiography film and the experiment cannot be tuned for varying types of radiation and intensity. However, the single particle digital autoradiography

technique (iQid), employed to analyze the Cast Stone samples in our study, is much more advantageous because it provides real-time imaging of individual radioactive decay events and is tunable to specific forms of radiation.

In the presented iQid images (Figure 4-9), the color scale for the images represents the relative number of β-decays measured at that individual pixel. Each pixel has a resolution of ~10 µm…Brian confirm. The brighter the signal in the image corresponds to a higher number of detected β-decays, and therefore a higher concentration of Tc, at that location. All images are presented with identical collection settings. An example of Tc detection and detection efficiency is shown in the Supplemental Information Figure S2.

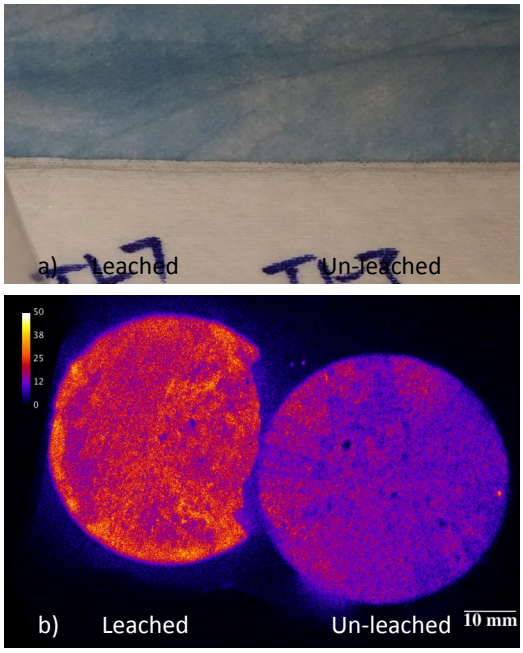

Figure 4 - a) photographs of the cross-sectioned pucks from the CS-Control monolith after 63 d leaching in VZPW and before leaching and b) the corresponding iQid images showing Tc distribution.

A cross section or "puck" was cut from the center of the Cast Stone samples before and after 63 d leaching. Figure 4 displays the iQid images collected from the CS-Control with the 63-d leached puck on the left side of the image. Photographs of the pucks are also presented for reference, the dark green interior observed in Figure 3 is not present on the puck surface due to air oxidation at the time of the photograph of the puck. In the iQid image of the unleached CS-Control, the β-decay signal is relatively evenly distributed throughout the sample. In the 63-d leached sample, the Tc remains distributed evenly in the sample although a stronger Tc signal arises from regions near the outer edge (between the 5 and 10 o'clock positions). This increased signal on the outer edge may be indication of a physical barrier to Tc transport from the outer wall carbonate deposit This distribution of Tc in the getter-free system demonstrates thorough

mixing during Cast Stone fabrication, ensuring a homogenous composition. Environmental modelling of release from waste forms also assumes a homogenous source. The brighter image in the 63-d leached sample may be due to the leaching process, and a combination of factors including the effect of water penetration into the monolith and the impact this has on both the porosity of the Cast Stone matrix and the Tc distribution. An increase in porosity would allow increased β decay events to reach the detector without being masked by a solid interface, thus the signal will appear stronger, even if the Tc concentration is similar, as a result of the increase in effective sampling volume of the iQid detector. This inhibits the ability to quantitatively compare images from one sample to another.

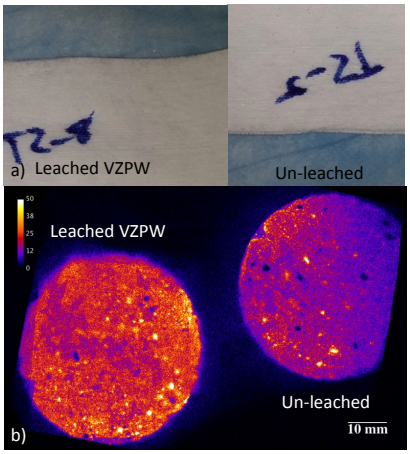

Figure 5 - a) photographs of the cross-sectioned pucks from the CS-Sn-A monolith after 63 d leaching in VZPW and before leaching and b) the corresponding iQid images showing Tc distribution.

The introduction of Tc getters to the Cast Stone has a large effect on Tc distribution within the sample. Figure 5 displays the iQid images collected from the CS-Sn-A pucks. In the unleached sample, distinct regions of higher signal, or "hot spots", are present throughout the sample corresponding to higher levels of Tc. Following leaching, the hot spots are still present with some congregating near the outer edge. A sample of the hot spot region was extracted from an unleached Sn-A Cast Stone monolith for further analysis. This sample was mounted in epoxy and imaged with the iQid, Figure 6 a). In the iQid image, several hot spots were observed. This activity map can then be correlated with additional elemental mapping using μ-XRF. One hot spot is highlighted by an arrow in the iQid image in Figure 6 b). This location also has an accumulation of Cr, a redox active constituent like Tc, as shown in the μ-XRF map in Figure 6 c). There are also prominent signals from P and Sn at this location in Figures 6 d) and e), arising from the residual Sn-A. This correlation between the position of the Tc, Cr, Sn and P demonstrates that redox-active species (Cr and Tc) removed from the LAW simulant by the Sn-A getter remain associated with the Sn-A getter in the Cast Stone matrix. At the top of the XRF map in Figure 6 d) and e), a large signal from P and Sn is present. This signal corresponds to the white area on the left edge of the sample in Figure 6 a). From the iQid image in Figure 6 b),

there was no Tc signal associated with this area, but there is a Tc signal coming from the area surrounding the white area, suggesting that Tc reacted with the surface of the getter and was not incorporated into the Sn-A structure.

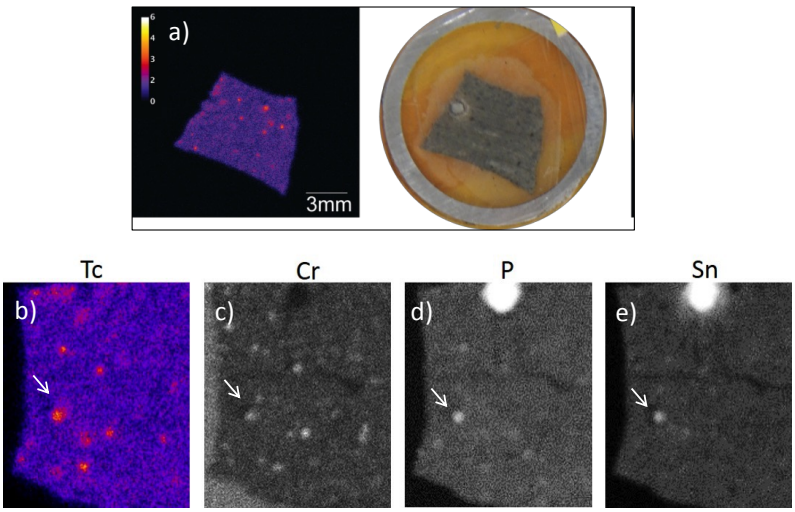

Figure 6 - a) iQid image and photograph of the sample extracted from the CS-Sn-A, b) magnified iQid image showing several Tc hot spots and the corresponding µ-XRF maps of c) Cr, d) P and e) Sn. The white arrow in b) – e) highlights the same spot in each image.

After identifying Tc "hot spots" in the vicinity of the Sn-A added as Tc getter within the Cast Stone matrix, pucks from the monoliths of CS-KMS-2 were also analyzed with the iQid (Figure 7). Tc hot spots are visible in the iQid image of the unleached KMS-2 Cast Stone and the hot spots remain even after leaching. Due to the smaller particle size and low amount of KMS-2 added, correlating the Tc hot spots to KMS-2 rich locations within Cast Stone matrix is challenging, given the 30µm resolution of the µ-XRF. A slice of the unleached KMS-2 Cast Stone was imaged with the iQid (Figure 8 a) and b). The corresponding elemental maps show some Cr isolations in the sample (Figure 8 c). Sn and S are the two largest components of the KMS-2 yet their XRF maps do not correlate to the Tc hot spots (Figures 8 d) and e). However, it is likely that the Tc is associated with the KMS-2 getter in the CS-KMS-2 based on circumstantial evidence. For example, Tc(VII) was entirely removed from the LAW simulant after KMS-2 addition, the Tc hot spots were only observed in the getter containing Cast Stone samples, and in the CS-Sn-A there is clear evidence that the Tc associated with the getter.

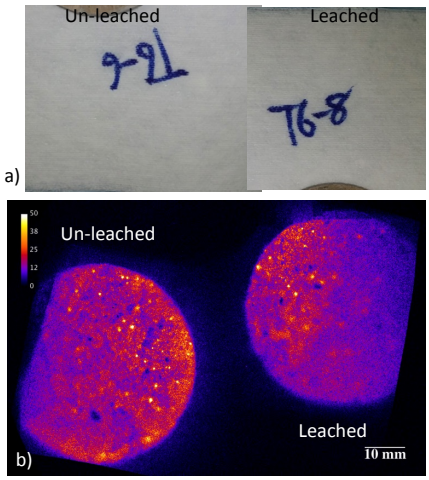

Figure 7 a) photographs of the cross-sectioned pucks from the CS-KMS-2 monolith after 63 d leaching in VZPW and before leaching and b) the corresponding iQid images showing Tc distribution.

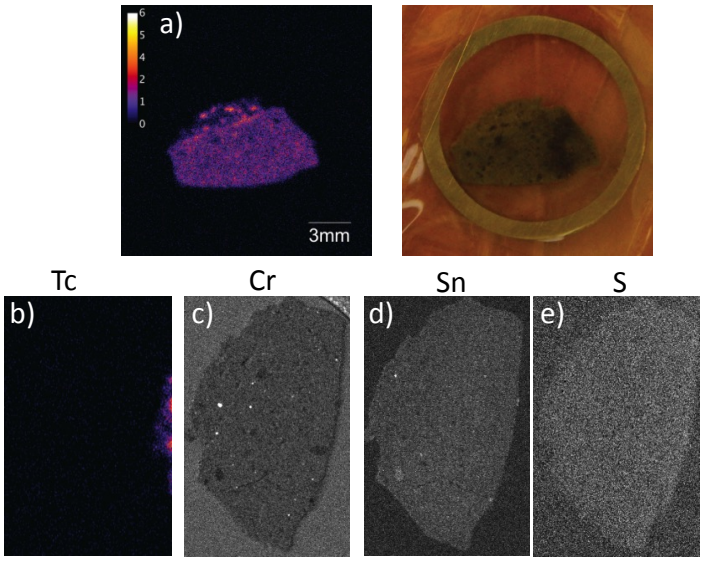

Figure 8 - a) iQid image and photograph of the sample extracted from the CS-KMS-2, b) magnified iQid image showing several Tc hot spots and the corresponding μ-XRF maps of c) Cr, d) Sn and e) S.

3.3.3 Influence of Tc oxidation state within Cast Stone

By remaining associated with the getters in the Cast Stone, the sequestered Tc will likely remain in the chemical state generated upon reaction with the getter. Sn-A has been shown to sequester Tc as a hydrated Tc-oxide, $Tc(IV)O_2 \cdot x\ H_2O$[35], while the KMS-2 generates a Tc-sulfide, $Tc(IV)_2S_7$ [36].

This difference in final Tc solid product could result in the differences in D_{obs} during leaching of the two Cast Stone systems. Analysis of a long-term (6 month) leached Cast Stone sample provides additional information the effect that Tc speciation has on Tc retention in the Cast Stone. Cast Stone samples were fabricated using a higher Tc spike of 56 ppm in the LAW, thus allowing Tc K-edge XANES analysis to determine oxidation state and local environment; however the Cast Stone composition remains unchanged. Results from the XAS analyses for the Cast Stone before and after 6 months leaching in VZPW are presented in Figure 9. Linear combination fitting of the XANES for the unleached sample (Figure 9 A) gave a Tc speciation of 59 % $Tc(VII)O_4^-$, 13 % of $Tc(IV)_2S_7$ and 28 % $Tc(IV)O_2$. After 6 months leaching (Figure 9 b), the Tc in the Cast Stone sample was composed of 76 % $Tc(VII)O_4^-$, 11 % of $Tc(IV)_2S_7$ and 13 % $Tc(IV)O_2$. The primary difference between the two samples was the increase in the $Tc(VII)O_4^-$ component and the decrease in $Tc(IV)O_2$ component for the 6 month leached sample, while the amount of $Tc(IV)_2S_7$ remained largely unchanged. This result shows that during the 6 month leaching period, the TcO_2 is preferentially re-oxidized to TcO_4^- and that the Tc_2S_7 is more resistant to re-oxidation to mobile TcO_4-. Previous analysis of cementitious based systems have revealed that BFS and the addition of FeS and NaS provided increased reduction of Tc(VII) within the waste form [54]. As the KMS-2 sequestered > 98% of the Tc from the LAW as Tc_2S_7, this Tc species will be more resistant to re-oxidation, thus slower to convert to mobile TcO_4^- leading to the improvement in diffusivity which was observed in the leach testing. Previous analysis of cementitious based systems have revealed that BFS and the addition of FeS and NaS provided increased reduction of Tc(VII) within the waste form.

Previous Tc getter inclusion in cementitious waste forms (67 % OPC and 33 % BFS) fabricated with a neutral simulated groundwater with lower Cr content and lower Tc spike (0.70 ppm) showed that both Sn-A and purolite resins were able to decrease Tc diffusivity[55]. In this work, we have demonstrated for the first time that a significant improvement in Tc retention and diffusivity is possible when minimal amounts of a Tc getter, e.g., KMS-2, are used to remove Tc from chemically extreme waste liquids with high pH, high ionic strength and in the presence of substantial amounts of competing redox sensitive elements, such as Cr. By selecting getters capable of sequestering Tc from the LAW environment, and by generating a more stable form towards re-oxidation of Tc, (e.g., Tc_2S_7), it is possible to retain the Tc with the getter in the cementitious waste form and decrease Tc leachability.

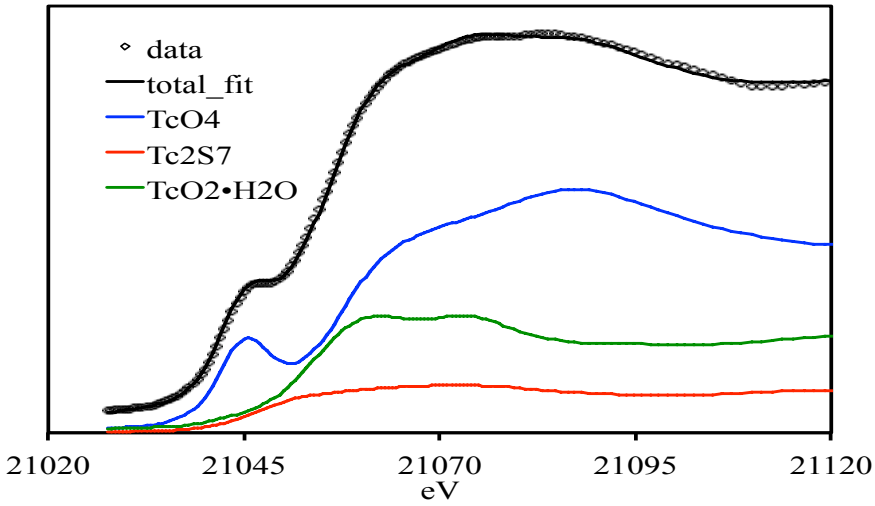

Figure 9 - Tc K-edge XANES spectrum and fit for the Cast Stone a) prior to leaching and b) after 6 month leaching in VZPW. The corresponding table shows the Tc K-edge fitting results for the Cast Stone samples analyzed. The numbers in parentheses represent the standard deviations of the contribution of that component for the ending digit, p is the probability that improvement of the fit, when this standard is included, is due to random error.

4.0 Conclusions

Two getter materials (Sn-A and KMS-2) were used in a pre-treatment contact step to remove Tc from simulated LAW prior to fabricating Cast Stone. The two getters were selected as each produced a different Tc final product: Tc(IV)-oxide via the Sn-A and Tc(IV)-sulfide via the KMS-2. Through a small addition of KMS-2 as a Tc getter (< 0.01 wt% of the total Cast Stone mass), > 98 % of the Tc was sequestered from the LAW. A higher addition of Sn-A was required to sequester 65 % of the Tc from the LAW. The sequestered Tc in the getter containing Cast Stone was identified to be primarily present as “hot spots” where it remained associated with the getter. The association of the Tc with the getters in the Cast Stone increased Tc retention in the solid and led to a significant reduction in the D_{obs} of Tc. The KMS-2 containing Cast Stone resulted in the largest decrease in Tc D_{obs} compared with Cast Stone without getters. Based on the results of this work, getters are a promising method to decrease contaminant release rates from cementitious waste forms fabricated with chemically extreme waste stream with minimal KMS-2 getter material addition.

Acknowledgements

Support for this project came from Washington River Protection Solutions. The authors wish to acknowledge the Kanatzidis group at Northwestern University for providing the KMS-2, RJ Lee Group (Richland, WA) for providing the Sn-Apatite, and Dave Swanberg (Washington River Protection Solutions, Supplemental Treatment Waste Form Development Project) for programmatic guidance, direction, and support. The authors acknowledge Ian Leavy, Erin McElroy, Steven Baum and Keith Geiszler for analyzing simulants and Cast Stone leachates.

SEM/EDS imaging was performed by Edgar Buck of PNNL. Tc K-edge XANES spectra were obtained at the Stanford Synchrotron Radiation Lightsource, SLAC National Accelerator Laboratory, which is supported by the U.S. Department of Energy, Office of Science, Office of Basic Energy Sciences under Contract No. DE-AC02-76SF00515. Cr L-edge XAS data were collected at the Advanced Light Source (ALS), Berkeley, which is supported by the Director, Office of Science, Office of Basic Energy Sciences (OBES) of the U.S. Department of Energy (DOE) under contract No. DE-AC02-05CH11231. A portion of this work (WWL) was supported by the U.S. Department of Energy, Office of Science, Basic Energy Sciences, Chemical Sciences, Biosciences, and Geosciences Division, Heavy Element Chemistry Program and was performed at Lawrence Berkeley National Laboratory under contract No. DE-AC02-05CH11231. The authors would like to thank Ben Williams for his expertise and assistance in Cast Stone monolith fabrication.

644 References

645 (1) Jones, L.; WM Symposia, 1628 E. Southern Avenue, Suite 9-332, Tempe, AZ
646 85282 (United States): 2013.
647 (2) Ojovan, M. I.; Lee, W. E. *Metallurgical and Materials Transactions A* **2011**, *42*,
648 837.
649 (3) Gin, S.; Abdelouas, A.; Criscenti, L. J.; Ebert, W. L.; Ferrand, K.; Geisler, T.;
650 Harrison, M. T.; Inagaki, Y.; Mitsui, S.; Mueller, K. T.; Marra, J. C.; Pantano, C. G.; Pierce, E.
651 M.; Ryan, J. V.; Schofield, J. M.; Steefel, C. I.; Vienna, J. D. *Materials Today* **2013**, *16*, 243.
652 (4) Kruger, A. A.; Kim, D. S. *Proceedings of WM2015* **2015**, *1167469*, Medium: ED.
653 (5) Polyakov, A. S.; Borisov, G. B.; Moiseenko, N. I.; Osnovin, V. I.; Dzekun, E. G.;
654 Medvedev, G. M.; Bel'tyukov, V. A.; Dubkov, S. A.; Filippov, S. N. *At Energy* **1994**, *76*, 181.
655 (6) Gephart, R. E. *Physics and Chemistry of the Earth, Parts A/B/C* **2010**, *35*, 298.
656 (7) Xu, K.; Hrma, P.; Rice, J. A.; Schweiger, M. J.; Riley, B. J.; Overman, N. R.;
657 Kruger, A. A. *Journal of the American Ceramic Society* **2016**, *99*, 2964.
658 (8) Zachara, J. M.; Serne, J.; Freshley, M.; Mann, F.; Anderson, F.; Wood, M.; Jones,
659 T.; Myers, D. *Vadose Zone Journal* **2007**, *6*, 985.
660 (9) Harrington, S.; Sams, T. *Proceedings of Waste Management Symposium* **2014**,
661 *2014*.
662 (10) Lenell, B. A.; Arai, Y. *Journal of Hazardous Materials* **2017**, *321*, 335.
663 (11) Langton, C. A. *Materials Research Society Symposium Proceedings* **1988**, *112*,
664 61.
665 (12) Faucon, P.; Adenot, F.; Jacquinot, J. F.; Petit, J. C.; Cabrillac, R.; Jorda, M.
666 *Cement and Concrete Research* **1998**, *28*, 847.
667 (13) Babaahmadi, A.; Tang, L.; Abbas, Z.; Zack, T.; Mårtensson, P. *Materials and*
668 *Structures* **2016**, *49*, 705.
669 (14) Swift, P.; Kinoshita, H.; Collier, N. C.; Utton, C. A. *Advances in Applied*
670 *Ceramics* **2013**, *112*, 1.
671 (15) Bird, G. W.; Lopata, V. J. In *Scientific Basis for Nuclear Waste Management*;
672 Northrup, C. J. M., Ed.; Springer US: Boston, MA, 1980, p 419.
673 (16) Palmer, D. A.; Meyer, R. E. *Journal of Inorganic and Nuclear Chemistry* **1981**,
674 *43*, 2979.
675 (17) Szecsody, J. E.; Jansik, D. P.; McKinley, J. P.; Hess, N. J. *Journal of*
676 *Environmental Radioactivity* **2014**, *135*, 147.
677 (18) Icenhower, J. P.; Qafoku, N. P.; Zachara, J. M.; Martin, W. J. *American Journal*
678 *of Science* **2010**, *310*, 721.
679 (19) Oostrom, M.; Truex, M. J.; Last, G. V.; Strickland, C. E.; Tartakovsky, G. D.
680 *Journal of Contaminant Hydrology* **2016**, *189*, 27.
681 (20) Westsik, J. H.; Piepel, G. F.; Lindberg, M. J.; Heasler, P. G.; Mercier, T. M.;
682 Russel, R. L.; Cozzi, A. D.; Daniel, W. E.; Eibling, R. E.; Hansen, E. K.; Reigal, M. R.;
683 Swanberg, D. J. *PNNL-22747, SRNL-STI-2013-00465* **2013**, *Rev. 0, Pacific Northwest National*
684 *Laboratory, Richland, Washington and Savannah River National Laboratory, Aiken, South*
685 *Carolina*.
686 (21) Westsik Jr, J.; Cantrell, K. J.; Serne, R. J.; Qafoku, N. *PNNL-23329, EMSP-RPT-*
687 *023* **2014**, *Pacific Northwest National Laboratory, Richland, WA*.
688 (22) Chung, C.-W.; Um, W.; Valenta, M. M.; Sundaram, S. K.; Chun, J.; Parker, K. E.;
689 Kimura, M. L.; Westsik Jr, J. H. *Journal of Nuclear Materials* **2012**, *420*, 164.

(23) EPA *Method 1315* **2013**, *US Environmental Protection Agency, Washington, DC*.
(24) Mattigod, S. V.; Fryxell, G.; Parker, K.; Kaplan, D. In *MRS Proceedings*; Cambridge Univ Press: 2002; Vol. 757, p II8. 7.
(25) Koivula, R.; Harjula, R. *Separation Science and Technology* **2010**, *46*, 315.
(26) Darab, J. G.; Amonette, A. B.; Burke, D. S. D.; Orr, R. D.; Ponder, S. M.; Schrick, B.; Mallouk, T. E.; Lukens, W. W.; Caulder, D. L.; Shuh, D. K. *Chemistry of Materials* **2007**, *19*, 5703.
(27) Wellman, D. M.; Mattigod, S. V.; Parker, K. E.; Heald, S. M.; Wang, C.; Fryxell, G. E. *Inorganic Chemistry* **2006**, *45*, 2382.
(28) Li, D.; Kaplan, D. I.; Knox, A. S.; Crapse, K. P.; Diprete, D. P. *Journal of Environmental Radioactivity* **2014**, *136*, 56.
(29) Levitskaia, T. G.; Chatterjee, S.; Pence, N. K.; Romero, J.; Varga, T.; Engelhard, M. H.; Du, Y.; Kovarik, L.; Arey, B. W.; Bowden, M. E.; Walter, E. D. *Environmental Science: Nano* **2016**.
(30) Sarri, S.; Misaelides, P.; Zamboulis, D.; Gaona, X.; Altmaier, M.; Geckeis, H. *J Radioanal Nucl Chem* **2016**, *307*, 681.
(31) Long, K. M.; Goff, G. S.; Ware, S. D.; Jarvinen, G. D.; Runde, W. H. *Industrial & Engineering Chemistry Research* **2012**, *51*, 10445.
(32) Qafoku, N.; Neeway, J. J.; Lawter, A. R.; Levitskaia, T. G.; Serne, R. J.; Westsik, J., J.H.; Valenta Snyder, M. M. *PNNL-23282* **2014**, *Pacific Northwest National Laboratory*.
(33) Neeway, J. J.; Qafoku, N.; Serne, R. J.; Lawter, A. J.; Stephenson, J. R.; Lukens, W. W.; Westsik Jr., J. H. *PNNL-23667* **2015**, *Pacific Northwest National Laboratory, Richland, Washington*.
(34) Neeway, J. J.; Lawter, A. R.; Serne, R. J.; Asmussen, R. M.; Qafoku, N. P. In *MRS Proceedings*; Cambridge Univ Press: 2015; Vol. 1744, p mrsf14.
(35) Asmussen, R. M.; Neeway, J. J.; Lawter, A. R.; Levitskaia, T. G.; Lukens, W. W.; Qafoku, N. *Journal Of Nuclear Materials* **2016**, *480*, 393.
(36) Neeway, J. J.; Asmussen, R. M.; Lawter, A. R.; Bowden, M. E.; Lukens, W. W.; Sarma, D.; Riley, B. J.; Kanatzidis, M. G.; Qafoku, N. P. *Chemistry of Materials* **2016**, *28*, 3976.
(37) Certa, P. J.; Empey, P. A. *ORP-11242* **2011**, *Revision 6, Washington River Protection Solutions, LLC, Richland, Washington*.
(38) Brown, C. F.; Serne, R. J.; Bjornstad, B. N.; Horton, D. G.; Lanigan, D. C.; Clayton, R. E.; Valenta, M. M.; Vickerman, T. S.; Kutnyakov, I. V.; Geiszler, K. N. *PNNL-15503, Rev. 1* **2006**, *Pacific Northwest National Laboratory (PNNL), Richland, WA (US)*.
(39) Um, W.; Yang, J.-S.; Serne, R. J.; Westsik, J. H. *Journal of Nuclear Materials* **2015**, *467, Part 1*, 251.
(40) Hassanzadeh Fard, Z.; Malliakas, C. D.; Mertz, J. L.; Kanatzidis, M. G. *Chemistry of Materials* **2015**, *27*, 1925.
(41) Mertz, J. L.; Fard, Z. H.; Malliakas, C. D.; Manos, M. J.; Kanatzidis, M. G. *Chemistry of Materials* **2013**, *25*, 2116.
(42) Miller, B. W.; Frost, S. H.; Frayo, S. L.; Kenoyer, A. L.; Santos, E.; Jones, J. C.; Green, D. J.; Hamlin, D. K.; Wilbur, D. S.; Fisher, D. R. *Medical physics* **2015**, *42*, 4094.
(43) Webb, S. M. *Physica Scripta* **2005**, *2005*, 1011.
(44) Ravel, B.; Newville, M. *Physica Scripta* **2005**, *2005*, 1007.
(45) Lukens, W. W.; Bucher, J. J.; Shuh, D. K.; Edelstein, N. M. *Environmental Science & Technology* **2005**, *39*, 8064.

(46) Haynes, W. M. *CRC handbook of chemistry and physics*; CRC press, 2014.
(47) Cobble, J. W.; Smith, W. T.; Boyd, G. E. *Journal of the American Chemical Society* **1953**, *75*, 5777.
(48) van Brakel, J.; Heertjes, P. M. *International Journal of Heat and Mass Transfer* **1974**, *17*, 1093.
(49) Atkinson, A.; Nelson, K.; Valentine, T. M. *Nuclear and Chemical Waste Management* **1986**, *6*, 241.
(50) Atkinson, A.; Nickerson, A. K. *Nuclear Technology* **1988**, *81*, 100.
(51) Cantrell, K. J.; Westsik Jr, J. H.; Serne, R. J.; Um, W.; Cozzi, A. D. *PNNL-25194* **2016**, *Pacific Northwest National Laboratory, Richland, WA*.
(52) DOE, U. S. D. o. E. *DOE/EIS-0391* **2012**, *Office of River Protection, U.S. Department of Energy, Richland, WA*.
(53) Dayal, R.; Davis, R. E.; Schweitzer, D. G. *BNL-NUREG-33580* **1983**, *Brookhaven National Laboratory, Upton, NY*.
(54) Allen, P. G.; Siemering, G. S.; Shuh, D. K.; Bucher, J. J.; Edelstein, N. M.; Langton, C. A.; Clark, S. B.; Reich, T.; Denecke, M. A. *Radiochimica Acta* **1997**, *76*, 77.
(55) Duncan, J. B.; Cooke, G. A.; Lockrem, L. L. *RPP-RPT-29195* **2009**, *Washington River Protection Solutions, Richland, WA, USA*.

Figure Captions

Table 1 – Composition of the LAW Simulant utilized in Cast Stone formation.

Table 2 – Composition of the simulated Hanford vadose zone pore water (VZPW) used in EPA Method 1315 leach testing.

Table 3 – Fabrication recipes for the Cast Stone samples used in this study.

Figure 1 – the percentage of initial concentration of a) Tc (16 ppm) and b) Cr (873 ppm) removed from the LAW simulant by the Tc getters prior to Cast Stone fabrication.

Figure 2 – a) the resulting Tc D_{obs} measured and b) the resulting Na D_{obs} values during the 63 d leaching period of the Cast Stone monoliths with and without Tc getters. The Cast Stone monoliths were leached in VZPW and placed into a fresh leachant at each interval at a sample surface area to leachate volume of 1 cm^2 : 9 mL. The errors bars represent the standard deviation of the mean on the two leaching samples.

Figure 3 – photographs of the Cast Stone monoliths in their cured form, opened after curing and following 63 d leaching for a) the control system with no getters, b) Sn-A containing Cast Stone and c) KMS-2 containing Cast Stone.

Figure 4 – a) photographs of the cross-sectioned pucks from the CS-Control monolith after 63 d leaching in VZPW and before leaching and b) the corresponding iQid images showing Tc distribution.

Figure 5 – a) photographs of the cross-sectioned pucks from the CS-Sn-A monolith after 63 d leaching in VZPW and before leaching and b) the corresponding iQid images showing Tc distribution.

Figure 6 – a) iQid image and photograph of the sample extracted from the CS-Sn-A, b) magnified iQid image showing several Tc hot spots and the corresponding μ-XRF maps of c) Cr, d) P and e) Sn. The white arrow in b) – e) highlights the same spot in each image.

Figure 7 – a) photographs of the cross-sectioned pucks from the CS-KMS-2 monolith after 63 d leaching in VZPW and before leaching and b) the corresponding iQid images showing Tc distribution.

Figure 8 – a) iQid image and photograph of the sample extracted from the CS-KMS-2, b) magnified iQid image showing several Tc hot spots and the corresponding μ-XRF maps of c) Cr, d) Sn and e) S.

Figure 9 - Tc K-edge XANES spectrum and fit for the Cast Stone A) prior to leaching and B) after 6 month leaching in VZPW. The corresponding table shows the Tc K-edge fitting results for the Cast Stone samples analyzed. The numbers in parentheses represent the standard deviations of the contribution of that component for the ending digit, p is the probability that improvement of the fit, when this standard is included, is due to random error.